

## Smoke over haze: Aircraft observations of chemical and optical properties and the effects on heating rates and stability

Brett F. Taubman

Department of Chemistry, The University of Maryland, College Park, Maryland, USA

Lackson T. Marufu, Brian L. Vant-Hull, Charles A. Piety, Bruce G. Doddridge, Russell R. Dickerson,<sup>1</sup> and Zhanqing Li

Department of Meteorology, The University of Maryland, College Park, Maryland, USA

Received 20 June 2003; revised 23 October 2003; accepted 13 November 2003; published 22 January 2004.

[1] Airborne observations made on 8 July 2002 over five locations in Virginia and Maryland revealed the presence of two discrete layers of air pollution, one of a smoke plume between  $\sim 2$  and 3 km above mean sea level advected from Quebec forest fires and another, underlying plume from fossil fuel combustion. Within the smoke layer, large increases were observed in submicrometer particle numbers, scattering, and absorption as well as ozone ( $O_3$ ) and CO (but not  $SO_2$ ) mixing ratios. The single-scattering albedos ( $\omega_0$ ) in the layer between  $\sim 2$  and 3 km (mean value at 550 nm =  $0.93 \pm 0.02$ ) were consistently smaller than those below (mean value at 550 nm =  $0.95 \pm 0.01$ ). Aerosol optical depth in the lower 3 km of the atmosphere was determined at each of the five locations, and the value at 550 nm varied between  $0.42 \pm 0.06$  and  $1.53 \pm 0.21$ .

Calculations of clear-sky aerosol direct radiative forcing by the smoke plume using an atmospheric radiative transfer code indicated that the forcing at the top of the atmosphere was small relative to the forcing at the surface. Thus atmospheric absorption of solar radiation was nearly equal to the attenuation at the surface. The net effect was to cool the surface and heat the air aloft. A morning subsidence inversion positioned the smoke in a dense enough layer above the planetary boundary layer that solar heating of the layer maintained the temperature inversion through the afternoon. This created a positive feedback loop that prevented vertical mixing and dilution of the smoke plume, thereby increasing the regional radiative impact.

*INDEX TERMS:* 0305 Atmospheric Composition and Structure: Aerosols and particles (0345, 4801); 0345 Atmospheric Composition and Structure: Pollution—urban and regional (0305); 0360 Atmospheric Composition and Structure: Transmission and scattering of radiation; *KEYWORDS:* smoke, aerosol, forcing, fire, radiation, heating

**Citation:** Taubman, B. F., L. T. Marufu, B. L. Vant-Hull, C. A. Piety, B. G. Doddridge, R. R. Dickerson, and Z. Li (2004), Smoke over haze: Aircraft observations of chemical and optical properties and the effects on heating rates and stability, *J. Geophys. Res.*, 109, D02206, doi:10.1029/2003JD003898.

### 1. Introduction

[2] In early July 2002, a pall of smoke, the result of forest fires in Quebec, blanketed the midatlantic and northeastern United States. An optically thick, subcontinental smoke plume can have significant impacts on regional air quality and the radiation budget. Large amounts of trace gases, including CO,  $NO_x$ , and ozone ( $O_3$ ), are typically associated with biomass combustion plumes [Evans *et al.*, 1977; Crutzen *et al.*, 1979; Stith *et al.*, 1981; Delmas, 1982; Crutzen and Andreae, 1990; Andreae and Merlet, 2001].  $O_3$  is photochemically produced downwind of fires in the presence of  $NO_x$ , nonmethane hydrocarbons, CO, and

UV light [Evans *et al.*, 1977; Stith *et al.*, 1981; McKeen *et al.*, 2002]. Combustion temperatures during biomass burning are not high enough to fix atmospheric nitrogen; rather, the reactive nitrogen generated from biomass burning results from the nitrogen content of the species burned [Andreae and Merlet, 2001]. Most of the species also contain S, but little  $SO_2$  is normally observed downwind of biomass burning [Stith *et al.*, 1981].

[3] Particles generated from burning vegetation are dominated by organic carbon (OC) and black carbon (BC) [Crutzen and Andreae, 1990; Martins *et al.*, 1998] that reduce the flux at the surface by scattering and absorbing solar radiation [Penner *et al.*, 1992; Hobbs *et al.*, 1997; Remer *et al.*, 1998; Eck *et al.*, 1998; Li, 1998; Li and Kou, 1998]. This is in contrast to sulfate particles, prevalent over the eastern United States, that predominantly scatter solar radiation and cool both the atmosphere and the surface [Charlson *et al.*, 1991; Ramanathan *et al.*, 2001]. The

<sup>1</sup>Also at Department of Chemistry, The University of Maryland, College Park, Maryland, USA.

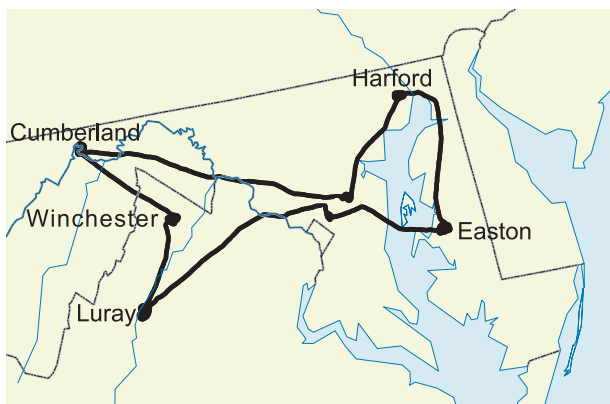


**Figure 1.** Flight track for 8 July 2002, consisting of a morning and an afternoon flight. Luray, Virginia (38.70°N, 78.48°W), Winchester, Virginia (39.15°N, 78.15°W), and Cumberland, Maryland (39.60°N, 78.70°W), (in that order chronologically) were the locations of the morning flight spirals. Harford, Maryland (39.56°N, 76.18°W), and Easton, Maryland (38.80°N, 76.06°W), (in that order chronologically) were the locations of the afternoon flight spirals.

degree of absorptivity of carbonaceous smoke particles depends largely on fuel type (dictated by region and vegetation), age of the particles, and the phase of burning (i.e., flaming versus smoldering) [Dubovik *et al.*, 2001].

Emissions from North American boreal forest fires have been shown to be less absorptive than those of African savannah and South American cerrado fires and commensurate with those of Amazonian forest fires [Dubovik *et al.*, 2001]. This is largely due to a protracted smoldering phase in forest fires that produces less absorptive particles. Chemical and physical transformations may, however, occur downwind of the source. In an aged plume, particle coagulation, gas-to-particle conversion, heterogeneous reactions, and cloud processing influence the trace gas concentrations and the size distribution and optical properties of the smoke particles [Reid *et al.*, 1998, 1999; Wong and Li, 2002]. Near source and downwind in situ measurements are thus necessary to provide constraints on remote sensing retrieval algorithms as well as for validations of numerical based model simulations.

[4] The scattering Ångström exponent,  $\alpha$ , a measure of the wavelength ( $\lambda$ ) dependence of the scattering coefficient, is inversely related to particle size, and thereby provides information on the source and age of the observed particles:

$$\alpha = \frac{-\log(\sigma_{sp\lambda_1}/\sigma_{sp\lambda_2})}{\log(\lambda_1/\lambda_2)}. \quad (1)$$

The single-scattering albedo ( $\omega_0$ ) is the ratio of particle scattering (represented by the scattering coefficient,  $\sigma_{sp}$ ) to total extinction due to particle scattering and absorption

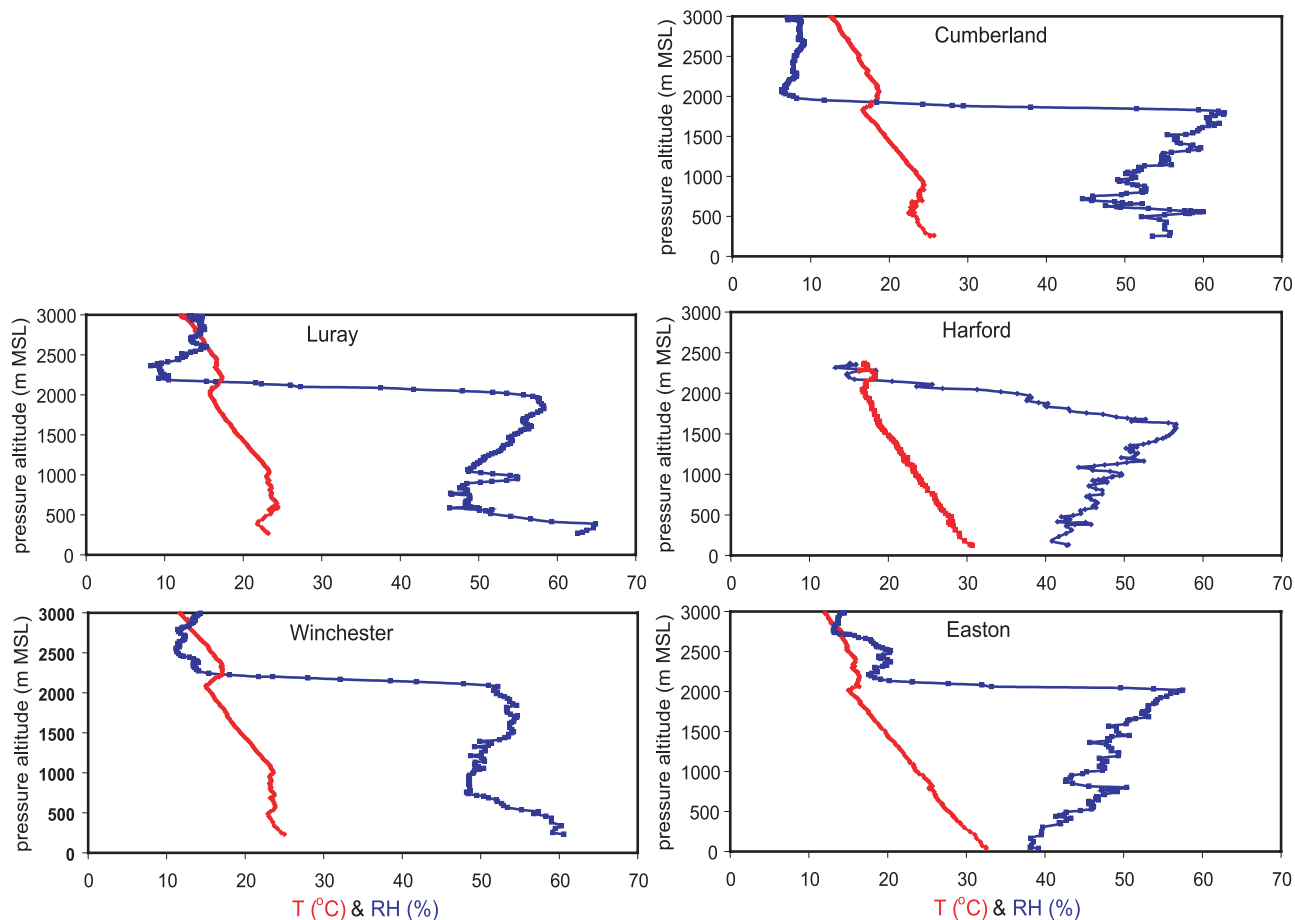


**Figure 2.** Measured temperature (red) and relative humidity (blue) over Luray, Winchester, Cumberland, Harford, and Easton.

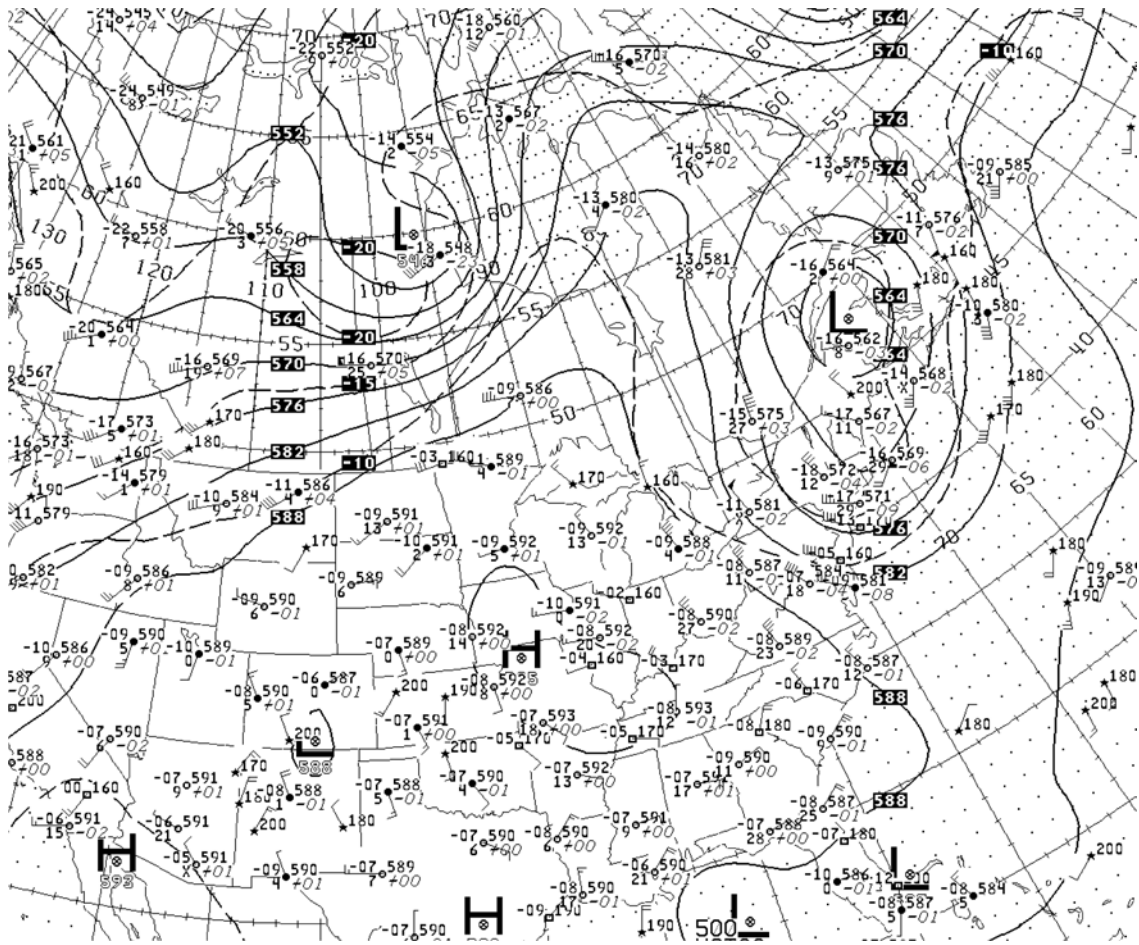


**Figure 3.** National Center for Environmental Prediction analysis of the geopotential height field at 500 mb for 1200 UTC, 6 July 2002.

(represented by the absorption coefficient,  $\sigma_{ap}$ ), and represents the probability that a photon encountering the particle will be scattered:

$$\omega_0 = \frac{\sigma_{sp}}{(\sigma_{sp} + \sigma_{ap})}. \quad (2)$$

[5] Smoke particles reportedly become less absorptive with age [Reid *et al.*, 1998]. In optically thick smoke plumes, small changes in  $\omega_0$  can have profound impacts on the radiative budget [Reid *et al.*, 1999]. The energy balance of the surface-atmosphere system is thus altered according to the degree of scattering and absorption [Eck *et al.*, 1998]. A more absorbing aerosol can heat the atmosphere and cool the surface, generating greater stability in the lower atmosphere and impacting the hydrological cycle [Ramanathan *et al.*, 2001]. This in turn affects the vertical mixing of the aerosols and potential removal mechanisms [e.g., Park *et al.*, 2001].

[6] The direct effect of aerosols upon this energy balance is quantified through calculations of aerosol direct radiative forcing. Top of the atmosphere forcing ( $\Delta F$  TOA) is a measure of the reflectivity of the atmosphere (after surface albedo is accounted for), while surface forcing ( $\Delta F$  sfc) gives the total attenuation of solar flux at the surface, both driven by aerosols in this case. If the two are equal, then the

aerosols are completely scattering. If the attenuation at the surface is greater than the reflected flux at the top of the atmosphere, then the aerosols have absorbed some of the solar radiation. Aerosol direct radiative forcing depends upon the aerosol optical depth (AOD,  $\tau$ ),  $\omega_0$ , and the asymmetry parameter ( $g$ ) of the particles. Aerosol optical depth is defined as the extinction coefficient,  $\sigma_{ext}$ , integrated from the surface (sfc) to the top of the atmosphere (TOA):

$$\tau(\lambda, RH) = \int_{sfc}^{TOA} \sigma_{ext}(\lambda, RH) dz. \quad (3)$$

The extinction coefficient is the sum of the scattering and absorption coefficients and  $\tau$  can therefore be represented as the sum of their vertical integrals:

$$\tau(\lambda, RH) = \int_{sfc}^{TOA} \sigma_{sp}(\lambda, RH) dz + \int_{sfc}^{TOA} \sigma_{ap}(\lambda, RH) dz. \quad (4)$$

The asymmetry parameter represents the degree of asymmetry of the angular scattering and is defined as

$$g = \frac{1}{2} \int_0^\pi \cos \theta P(\theta) \sin \theta d\theta \quad (5)$$



**Figure 4.** Moderate-Resolution Imaging Spectroradiometer (MODIS) visible image from the Terra satellite on 7 July 2002. Active fire detections are shown as red dots east of James Bay. Diffluence downstream of the upper-level trough caused the smoke plume to fan out over the eastern United States.

where  $\theta$  is the scattering angle and  $P$  is the phase function, the scattered intensity at angle  $\theta$  relative to the incident beam.

[7] Results of aircraft measurements of trace gas and particle concentrations as well as particle optical properties on 8 July 2002 over Maryland and Virginia are reported herein. The sampling methods and analytical techniques are described in detail. The AOD, aerosol direct radiative forcing, and heating rates associated with the smoke plume advected from Quebec forest fires are calculated. This paper also investigates the impacts that absorptive heating within the plume had on atmospheric stability.

## 2. Sampling Platform

[8] The sampling platform used for this study was a twin engine Piper Aztec-F PA-23-250 research aircraft. The aircraft is outfitted with a suite of trace gas and aerosol instruments, the inlets for which are engineered onto the upper fuselage. There is an aft-facing inlet plumbed to the trace gas instruments while a forward facing, isokinetic inlet feeds the aerosol instruments. Owing to inlet sampling line losses of supermicrometer particles, all measurements reported are of submicrometer particles only. A meteorological probe is nestled between these two inlets. Position

was measured and stored using a Global Positioning System, GPS (Garmin GPS-90), with 10 s resolution, and verified several times per flight relative to known geographic reference points. Temperature and relative humidity (RH) were measured using a thermistor and capacitive thin film, respectively, with a regularly calibrated Rustrak RR2-252 RH probe (EIL Instruments Inc., Hunt Valley, Maryland). The instrument is capable of 0.5°C temperature precision and 2% humidity precision with a 10 s response time. Pressure was measured using a Rosemount Model 2008 pressure transducer, capable of 5 mb precision, and calibrated regularly to a laboratory standard. Pressure altitude was calculated from static pressure using the U.S. Standard Atmosphere (1976) approximation, normalized relative to known surface elevation and ambient surface static pressure averaged between takeoff and landing locations.

[9] Ozone data were acquired with a commercial instrument using UV absorption at 254 nm (Thermo Environmental, TEI Model 49, Franklin, Massachusetts), modified for increased (4 s) temporal response. This instrument was routinely compared to an in-house primary O<sub>3</sub> calibrator (TEI Model 49PS) fed on zero-grade air.

[10] For observations of CO, a high-performance, modified [Dickerson and Delany, 1988] commercial (TEI Model 48) nondispersive infrared (NDIR) gas filter correlation analyzer was used. For this study, this instrument had a detection limit of  $\sim 24$  ppbv (signal to noise, S:N = 1:1 for  $\pm 2\sigma$  noise) for a 1 min mean of 10 s data, and was calibrated regularly using CO working standards (1–2 ppmv CO in nitrogen; Scott-Marrin, Riverside, California), in turn referenced to a National Institute of Standards and Technology (NIST) Standard Reference Material (1677c 9970 ppbv CO in nitrogen, certified; NIST, Gaithersburg, Maryland). This instrument is capable of  $\sim 1\%$  precision determined for a 1 min mean of 10 s data. The CO instrument has undergone formal international calibrations [Novelli et al., 1998] under a WMO protocol [Doddridge et al., 1995].

[11] A modified [Luke, 1997] commercial pulsed fluorescence detector (TEI Model 43C) was used for measurements of ambient SO<sub>2</sub>. For this experiment, the SO<sub>2</sub> instrument had a detection limit of  $\sim 140$  pptv (S:N = 1:1 for  $\pm 2\sigma$  noise) for a 1 min mean of 10 s data and was calibrated regularly using SO<sub>2</sub> working standards.

[12] Particle light absorption was measured using a Particle/Soot Absorption Photometer (PSAP, Radiance Research, Seattle, Washington), which quantified the intensity of 565 nm light after it passed through a filter on which ambient aerosol was deposited. The detection limit (95% confidence level) for S:N = 1 is  $0.9 \times 10^{-6} \text{ m}^{-1}$  [Anderson et al., 1999; Bond et al., 1999] when 1 min measurement averages are used as in this experiment. Absorption values were corrected for differences in flow rate (as measured by the instrument and an electronic bubble flow meter) and spot size, instrumental variation, noise, and exaggerations of absorption due to scattering and nonscattering influences [Bond et al., 1999]. These corrections resulted in a decrease in absorption values from those indicated by the instrument from approximately 10% for the smaller values to almost 20% for the larger ones. The estimated instrumental uncertainty for the absorption values is 25% with 95% confidence.

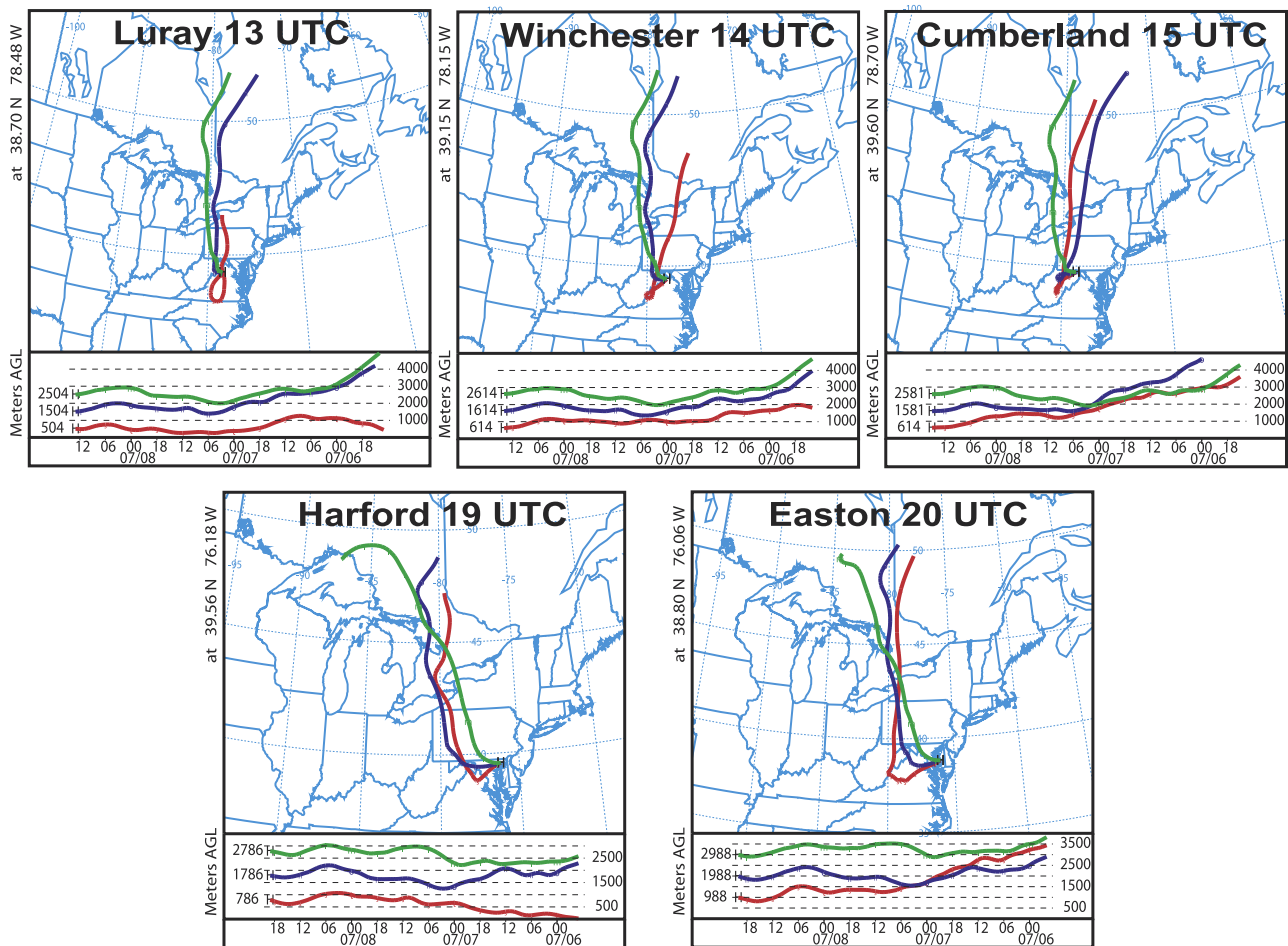


**Figure 5.** National Oceanic and Atmospheric Administration (NOAA) Air Resources Laboratory (ARL) Hybrid Single-Particle Lagrangian Integrated Trajectory (HY-SPLIT) model vertical velocity 72 hour backward trajectories using Eta Data Assimilation System (EDAS) meteorological fields at 1000, 2000, and 3000 m mean sea level on 8 July 2002 over Luray, Winchester, Cumberland, Harford, and Easton.

[13] Particle light scattering was quantified using an integrating nephelometer (TSI Model 3563) that measured the total particle scattering coefficient ( $\sigma_{sp}$ ) at 450, 550, and 700 nm [Anderson *et al.*, 1996]. The nephelometer was calibrated with  $\text{CO}_2$  and particle-free air, and corrected as necessary. At an averaging time of 5 min, detection limits for S:N = 2 are  $\sigma_{sp450} = 0.44 \times 10^{-6} \text{ m}^{-1}$ ,  $\sigma_{sp550} = 0.17 \times 10^{-6} \text{ m}^{-1}$ , and  $\sigma_{sp700} = 0.26 \times 10^{-6} \text{ m}^{-1}$ . Corrections were made to the measurements to account for forward scattering angular truncation and non-Lambertian distribution of illumination intensity within the nephelometer. A wavelength-dependent correction factor ( $C_{ts}$ ) was calculated assuming a linear relationship between  $C_{ts}$  and the scattering Ångström exponent ( $\alpha$ ), such that  $C_{ts} = a + b\alpha$ , where  $a$  and  $b$  are constants used for submicrometer particles and  $\alpha_{450/550}$ ,  $\alpha_{450/700}$ , and  $\alpha_{550/700}$  are used for 450, 550, and 700 nm, respectively [Anderson and Ogren, 1998]. Application of this correction increased the scattering values from  $\sim 5\%$  at 700 nm for the planetary boundary layer (PBL) particles to nearly 15% at 450 nm for the particles in the smoke plume. The estimated instrumental uncertainty for values of total scattering is 10% with 95% confidence.

[14] Number distributions for particles with optical diameters between 0.30 and 1.0  $\mu\text{m}$  were collected with an

optical particle counter (Met One Model 9012) that used a laser diode-based optical sensor to convert scattered light to numbers of particles per size range. The prespecified size ranges were 0.30–0.40  $\mu\text{m}$ , 0.40–0.491  $\mu\text{m}$ , 0.491–0.60  $\mu\text{m}$ , 0.60–0.701  $\mu\text{m}$ , 0.701–0.80  $\mu\text{m}$ , and 0.80  $\sim$  1.0  $\mu\text{m}$ .

### 3. Results and Discussion

[15] Two research flights, one in the morning and one in the afternoon, were conducted on 8 July 2002 (Figure 1). The dark black circles on the figure indicate ascending or descending fixed location vertical survey spirals performed at  $\sim 100 \text{ vertical m min}^{-1}$  between  $\sim 5 \text{ m}$  above ground level (AGL) to  $\sim 3 \text{ km}$  above mean sea level (MSL). The first spiral was made over Luray, Virginia ( $38.70^\circ\text{N}$ ,  $78.48^\circ\text{W}$ ) beginning at  $\sim 1300 \text{ UTC}$ . After a short transect to the northeast, the second spiral was performed over Winchester, Virginia ( $39.15^\circ\text{N}$ ,  $78.15^\circ\text{W}$ ) commencing at  $\sim 1400 \text{ UTC}$ . The final spiral of the morning, over Cumberland, Maryland ( $39.60^\circ\text{N}$ ,  $78.70^\circ\text{W}$ ) was initiated at  $\sim 1500 \text{ UTC}$ . The afternoon spirals were performed over Harford County (Harford), Maryland ( $39.56^\circ\text{N}$ ,  $76.18^\circ\text{W}$ ) and Easton, Maryland ( $38.80^\circ\text{N}$ ,  $76.06^\circ\text{W}$ ) beginning at  $\sim 1900$  and

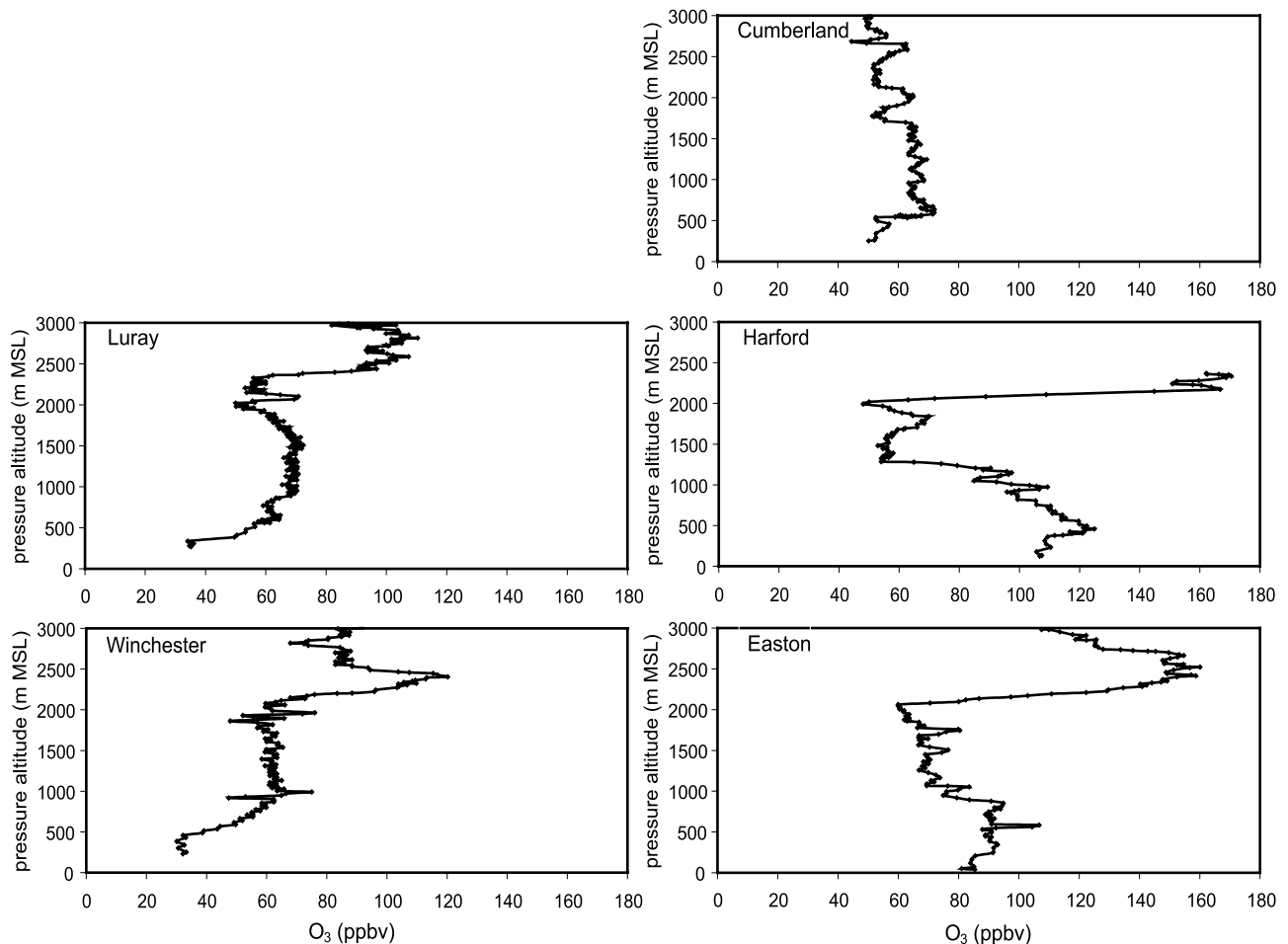


**Figure 6.** Ozone (10 s) measured during the vertical survey spirals over Luray, Winchester, Cumberland, Harford, and Easton.

2000 UTC, respectively. Evidence of the smoke plume was strongest over Luray, Winchester, Harford, and Easton. The spiral over Cumberland showed little evidence of the smoke plume. A backward trajectory analysis will be discussed in section 3.2.

[16] Vertical profiles of the temperature and RH measured over the five locations are given in Figure 2. The three morning profiles (Luray, Winchester, and Cumberland) show a nocturnal radiance inversion around 500 m that erodes by the time of the later profiles. A persistent inversion around 2 km is evident in all of the profiles, delineating the upper limits of the PBL and the dichotomy between the two regimes observed in this study. In this paper we investigate the hypothesis that absorption of solar radiation within the layer between  $\sim 2$  and 3 km led to the protraction of this temperature inversion, initiated by morning subsidence, through the afternoon.

### 3.1. Meteorology

[17] A cutoff upper-level low-pressure system centered over Maine, together with a high-amplitude ridge to the west, caused long range funneling of northern continental air to the midatlantic region beginning on 5 July 2002 and continuing through the morning of 8 July (Figure 3). This meridional flow is normally associated with cool, dry, and

relatively clean air. However, smoke from forest fires burning in northern Quebec traveled south over 1000 km to blanket the midatlantic and northeastern United States in a thick pall. Diffluence downstream of the upper-level trough caused the plume to fan out over the region. Figure 4 is a Moderate-Resolution Imaging Spectroradiometer (MODIS) visible image of the plume and several active fire detections (red dots) on 7 July that shows how the diffluent flow caused such a regional impact.

[18] On 8 July, the upper-level trough filled and migrated east, resulting in a wind shift to the west. This began to push the plume out over the Atlantic Ocean. By the 9th the majority of the plume was advected offshore. For a more complete analysis of the meteorology associated with this event, see [http://www.atmos.umd.edu/~forecaster/summary\\_2002.htm](http://www.atmos.umd.edu/~forecaster/summary_2002.htm).

### 3.2. Trajectory Analysis

[19] A backward trajectory analysis utilizing the NOAA Air Resources Laboratory (ARL) Hybrid Single-Particle Lagrangian Integrated Trajectory (HY-SPLIT) model (Version 4) (R. R. Draxler and G. D. Rolph, 2003, <http://www.arl.noaa.gov/ready/hysplit4.html>) and Eta Data Assimilation System (EDAS) meteorological fields was performed at each of the five locales addressed in this study

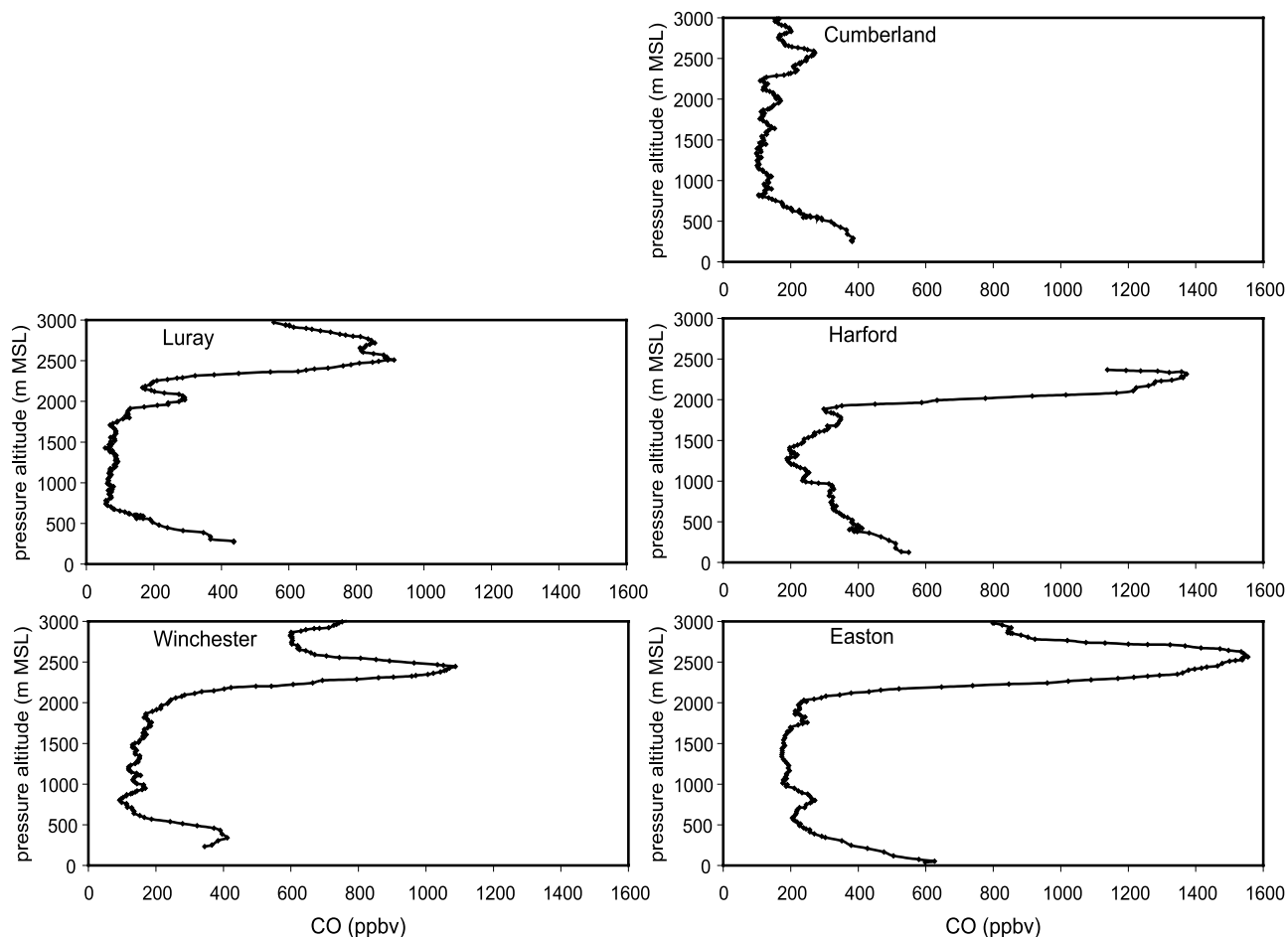


**Figure 7.** Running 1 min mean CO measured during the vertical survey spirals over Luray, Winchester, Cumberland, Harford, and Easton.

(Figure 5). The 72 hour model vertical velocity backward trajectories were commenced at altitudes of 1000, 2000, and 3000 m MSL to shed light on observations made within the PBL and the observed free tropospheric pall. The upper-level trajectories all show advection from the north and northwest, indicating that the observations between 2 and 3 km MSL were of the Canadian forest fire smoke. The meteorological and trajectory analyses suggest that air parcels were lifted near the fires and then transported in the lower free troposphere. The lower-level trajectories also show northerly advection, however the observations made in this study suggest a vertical separation between PBL air and that in the free troposphere.

### 3.3. Trace Gases

[20] The mixing ratios for  $O_3$ , CO, and  $SO_2$  measured over the five locations are provided in Figures 6, 7, and 8, respectively. Luray, Winchester, Harford, and Easton displayed similar trends: high  $O_3$  and CO mixing ratios between 2 and 3 km with little  $SO_2$  observed within this altitude range.  $O_3$  mixing ratios exceeded 160 ppbv at this altitude and the mixing ratios in the layer aloft consistently exceeded those in the PBL by 40–60 ppbv. CO mixing ratios approached 1600 ppbv in the layer aloft, and were upward of 1000 ppbv greater than those in the PBL. These observations are indicative of a photochemically aged

smoke plume. Large amounts of  $SO_2$  were observed near the surface in the three later profiles, including Cumberland. This enhanced  $SO_2$ , routinely observed during regular air pollution survey flights conducted in this area [Ryan *et al.*, 1998], could be the result of westerly transport from a point source, observed in the later profiles because of the wind shift from the north to the west.

### 3.4. Aerosol Properties

[21] Particle scattering at 450, 550, and 700 nm, absorption at 550 nm, and size number distributions for the six accumulation mode size bins over the five locations are provided in Figures 9, 10, and 11, respectively. The absorption values were extrapolated from 565 to 550 nm, based on the assumption that  $\sigma_{ap} \propto (1/\lambda)$  [Bodhaine, 1995], to calculate the AOD and single-scattering albedo at this wavelength. Methods used to extrapolate measured optical properties across the solar spectrum will be addressed later in this section. Total scattering at 450, 550, and even at 700 nm over Harford and Easton, exceeded  $10^{-3} m^{-1}$  between 2 and 3 km. Particle absorption at 550 nm approached  $100 Mm^{-1}$  in this vertical layer over each location and even surpassed this value at Easton. The greatest numbers of particles were observed in the 0.30–0.60  $\mu m$  diameter range. Particles larger than this may not have been collected efficiently due to inlet line losses. There

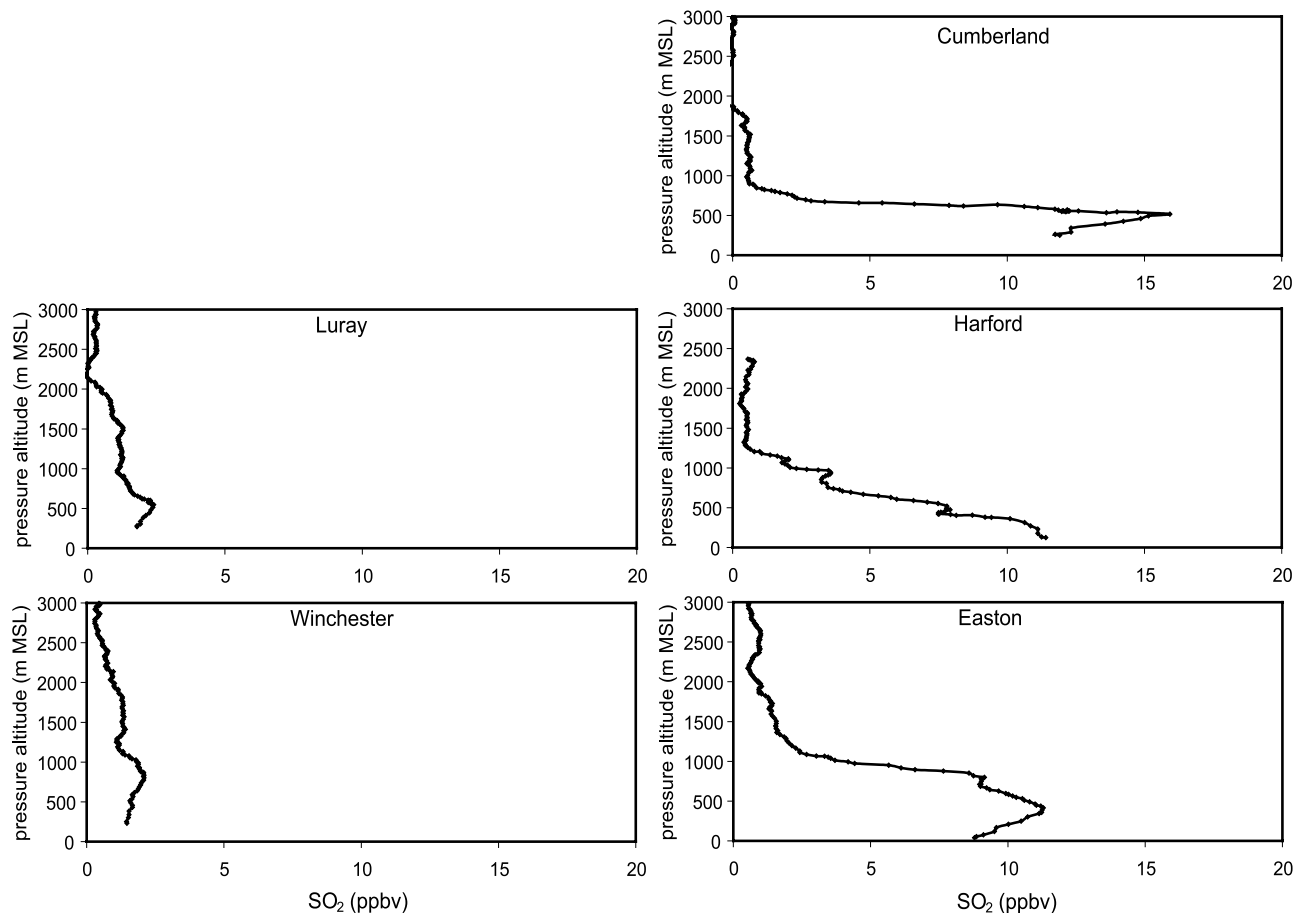


**Figure 8.** Same as Figure 7, but for  $\text{SO}_2$ .

were at least as many particles in the  $0.40\text{--}0.491\ \mu\text{m}$  range as in the smallest size bin observed over each location (except Cumberland and Harford) at  $\sim 2.5\ \text{km}$ , roughly the vertical center of the smoke plume. At Luray and Winchester, particles with diameters between  $0.491\text{--}0.60\ \mu\text{m}$  were also as numerous as those in the smallest size bin. These observations are rare in a typical plume of anthropogenic origin. In such cases, the particles with diameters between  $0.30\text{--}0.40\ \mu\text{m}$  are far more numerous than the larger particles, as can be seen in the PBL in the morning profiles.

[22] A large increase in the number of particles between  $0.30\text{--}0.40\ \mu\text{m}$  was seen at roughly  $500\ \text{m}$  above Cumberland. This increase corresponded to an increase in  $\text{SO}_2$  at the same altitude over Cumberland. Despite the fact that similar increases in  $\text{SO}_2$  were measured at low altitudes over Harford and Easton, no increase in the number of  $0.30\text{--}0.40\ \mu\text{m}$  particles was observed. The optically thick layer of smoke covering Harford and Easton may have inhibited the photooxidation of  $\text{SO}_2$  to  $\text{SO}_4^{2-}$  and thereby secondary aerosol formation. Over Cumberland, where there was less solar attenuation, gas to particle conversion would not have been hindered. This may have resulted in the observed increase in small particles. Unfortunately, there was no speciation data to confirm this supposition.

[23] Calculations of  $\alpha$  were made using the following ratios of the total scattering at  $450, 550,$  and  $700\ \text{nm}$ :  $450/550, 450/700,$  and  $550/700$ . Figure 12 shows  $\alpha_{450/700}$  over the five locations. Table 1 gives the average values of  $\alpha$  for

the smoke layer and the PBL at each location. The average values of  $\alpha$  in the PBL are larger than those in the smoke layer, indicating smaller particles in the PBL and larger ones aloft. This is consistent with relatively fresh anthropogenic particles lying below an aged smoke plume that had traveled over  $1000\ \text{km}$  [Reid *et al.*, 1998]. Even the Cumberland profile, despite showing a weak overall smoke signature, is consistent with this trend.

[24] Measurements of light scattering were made after the sample airflow was dried from ambient conditions to an RH of  $\leq 20\%$ . Measurements of light absorption were performed at ambient conditions. Although it was assumed in this study that changes in RH did not affect absorption, it has been shown that RH variations can cause inaccuracies in measurements made by the PSAP [Anderson *et al.*, 2003]. Because of the measurement of dry light scattering,  $\sigma_{\text{sp}}(\text{ref})$ , the calculation of AOD must be modified to account for the difference between  $\sigma_{\text{sp}}(\text{ref})$  and  $\sigma_{\text{sp}}(\lambda, \text{RH})$ :

$$\tau(\lambda, \text{RH}) = \int_{\text{sfc}}^{\text{TOA}} \sigma_{\text{sp}}(\text{ref}) F(\text{RH}) dz + \int_{\text{sfc}}^{\text{TOA}} \sigma_{\text{ap}}(\lambda, \text{RH}) dz, \quad (6)$$

where

$$F(\text{RH}) = \frac{\sigma_{\text{sp}}(\lambda, \text{RH})}{\sigma_{\text{sp}}(\text{ref})}. \quad (7)$$

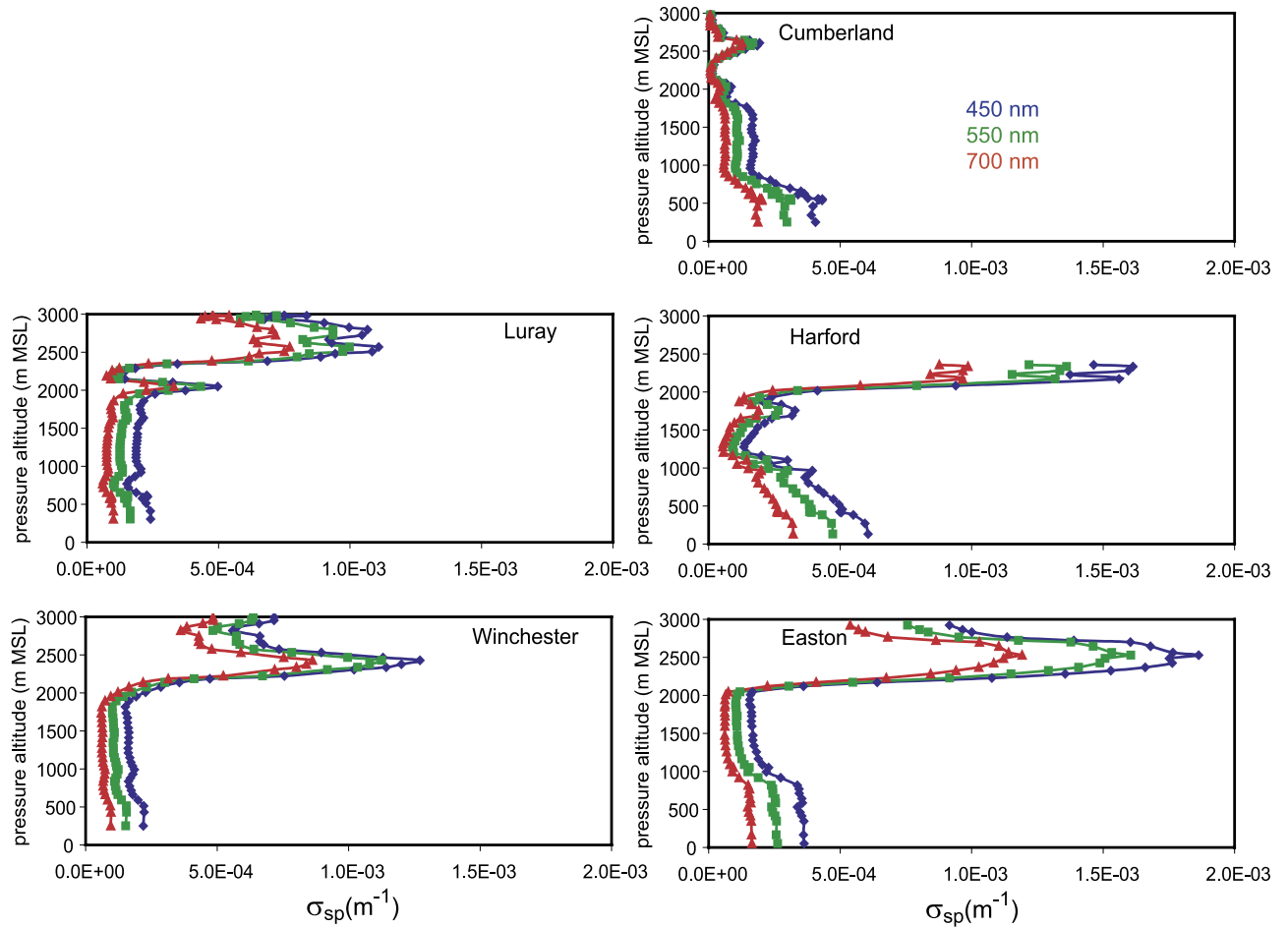


**Figure 9.**  $\sigma_{sp}$  at 450 nm (blue), 550 nm (green), and 700 nm (red) measured during the vertical survey spirals over Luray, Winchester, Cumberland, Harford, and Easton.

$F(\text{RH})$  was then calculated using the following relationship between particle scattering coefficients at two values of RH:

$$\frac{\sigma_{sp}(\lambda, \text{RH})}{\sigma_{sp}(\text{ref})} = \left( \frac{1 - \text{RH}_{\text{amb}}}{1 - \text{RH}_{\text{ref}}} \right)^{-\gamma}, \quad (8)$$

where  $\text{RH}_{\text{amb}}$  is the ambient RH,  $\text{RH}_{\text{ref}}$  is the RH inside the nephelometer, and  $\gamma$  is an empirically derived constant.

[25] Parallel nephelometers were not used in this study, so  $\gamma$  had to be estimated. In polluted conditions, such as those on the east coast of the United States, typical values of  $\gamma$  range from 0.20–0.50. For this study a value of 0.35 was chosen as per *Remer et al.* [1997] because of the similarities of both the sampling platforms and the regions of the studies. However, this correction factor was only applied to total scattering measurements made within the PBL. The smoke plume was presumably less hygroscopic than the sulfate dominated anthropogenic aerosols of the midatlantic United States and was observed in the free troposphere, where the RH was already below 20%. The corrections for angular nonidealities, on the other hand, were applied to all of the measurements.

[26] The vertical survey spirals covered roughly the bottom 3 km of the atmosphere, from  $\sim 5$  m AGL ( $z_1$ ) to  $\sim 3$  km MSL ( $z_2$ ). Because of the small temporal and

horizontal spatial scale of the individual spirals, atmospheric homogeneity was assumed in both horizontal composition and time. Thus AOD for the vertical column at a single time was calculated. Measurements of extinction (as the sum of scattering and absorption) were made every minute and roughly every 100 m to give approximately 30 measurements per spiral. These extinction measurements were then integrated vertically and the AOD reported herein was calculated as such:

$$\tau(\lambda, \text{RH}) = \int_{z_1}^{z_2} \sigma_{sp}(\text{ref}) F(\text{RH}) dz + \int_{z_2}^{z_2} \sigma_{ap}(\lambda, \text{RH}) dz. \quad (9)$$

The smoke plume was observed in the lower free troposphere at a minimum altitude of  $\sim 2$  km MSL and extended somewhat beyond 3 km MSL. Therefore the entire smoke plume was not accounted for in these calculations. AOD at 550 nm ( $\tau_{550}$ ) is given in Table 2. The uncertainty in these values was calculated by adding in quadrature the uncertainties in the particle scattering and absorption. A 25% uncertainty was assigned to the absorption values according to the instrumental error. A 15% uncertainty was estimated for the scattering values after adding in quadrature the 10% instrumental error and an additional 11% sensitivity to the possible range of  $\gamma$  values.

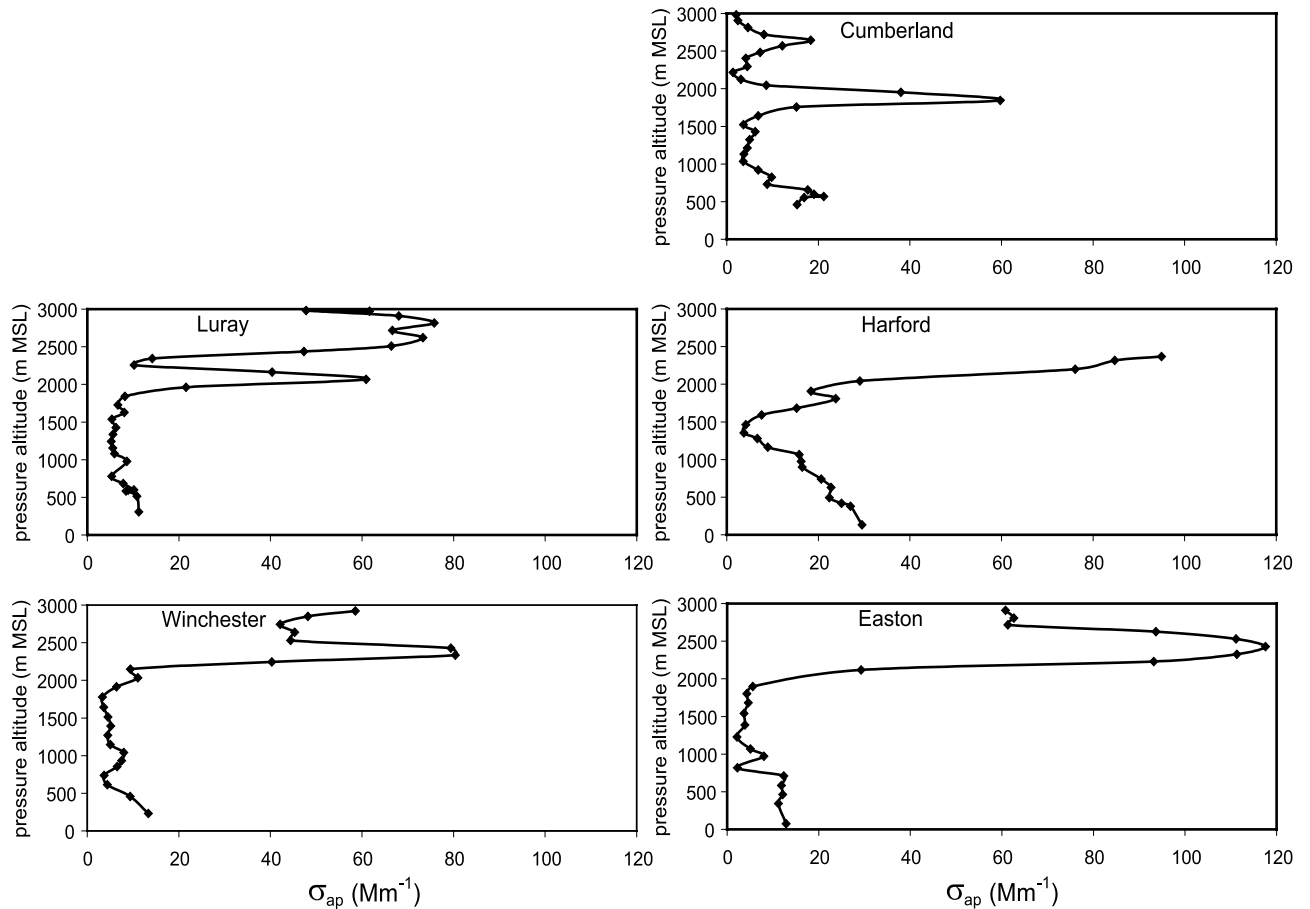


**Figure 10.**  $\sigma_{ap}$  at 550 nm, extrapolated from  $\sigma_{ap}$  at 565 nm, that was measured during the vertical survey spirals over Luray, Winchester, Cumberland, Harford, and Easton.

[27] The profiles of  $\omega_0$  at 550 nm ( $\omega_{0,550}$ ) over the five locations are given in Figure 13. The average values of  $\omega_{0,550}$  in the PBL and smoke layer aloft at each location are given in Table 3. The particles in the smoke plume were consistently more absorbing than the particles in the PBL. The mean values in the smoke plume and the PBL at 550 nm were  $0.93 \pm 0.02$  and  $0.95 \pm 0.01$ , respectively. Calculation of the mean smoke value excluded Cumberland. A weak smoke signature was observed over this location, and inclusion would bias the calculation toward a value uncharacteristic of the smoke plume measured over the other sites. These  $\omega_{0,550}$  values are consistent with those reported by Dubovik *et al.* [2001] for North American boreal forest fires and at NASA GSFC. The smoke plume values also fall within the range of satellite-based retrieved values for smoke from boreal forest fires [Ferrare *et al.*, 1990; Li and Kou, 1998]. The uncertainty in  $\omega_0$  was calculated according to the aforementioned uncertainties in the absorption and scattering values with the following equation:

$$\frac{|\Delta\omega_0|}{\omega_0} = (1 - \omega_0) \left[ \left( \frac{\Delta\sigma_{sp}}{\sigma_{sp}} \right)^2 + \left( \frac{\Delta\sigma_{ap}}{\sigma_{ap}} \right)^2 \right]^{\frac{1}{2}}. \quad (10)$$

[28] The wavelength-dependent indices of refraction and particle size distributions were necessary to extrapolate optical properties at the measured wavelengths over the

solar spectrum using Mie theory [Mishchenko *et al.*, 2002]. The real indices of refraction at 550 nm were determined assuming the column integrated AERONET (Aerosol Robotic Network) [Holben *et al.*, 1998] value at 550 nm (1.56, interpolated from the wavelengths measured) on 8 July 2002 represented a weighted average of two discrete values, one for the PBL plume and one for the smoke plume. The value assigned to the PBL plume was 1.43 according to a 7 year average from NASA GSFC in Greenbelt, Maryland [Dubovik *et al.*, 2001]. A value of 1.58 was therefore assigned to the smoke plume, slightly larger than the column integrated value. These refractive indices were then scaled according to the wavelength dependence of the AERONET values. The imaginary indices of refraction were calculated assuming absorption was solely the result of particle BC content. The wavelength dependence was then considered to be proportional to that measured for BC [Chang and Charalampopolous, 1990], adjusted so the  $\omega_0$  value calculated at 550 nm matched the in situ value.

[29] The measured particle size distributions were over a limited size range. Thus size distributions were determined using the measured Ångström exponents and the assumed complex indices of refraction at 550 nm. The lognormal distributions were adjusted so that the Ångström exponents calculated from Mie theory matched the measured values. Optical properties ( $\omega_0$ , phase functions) at other

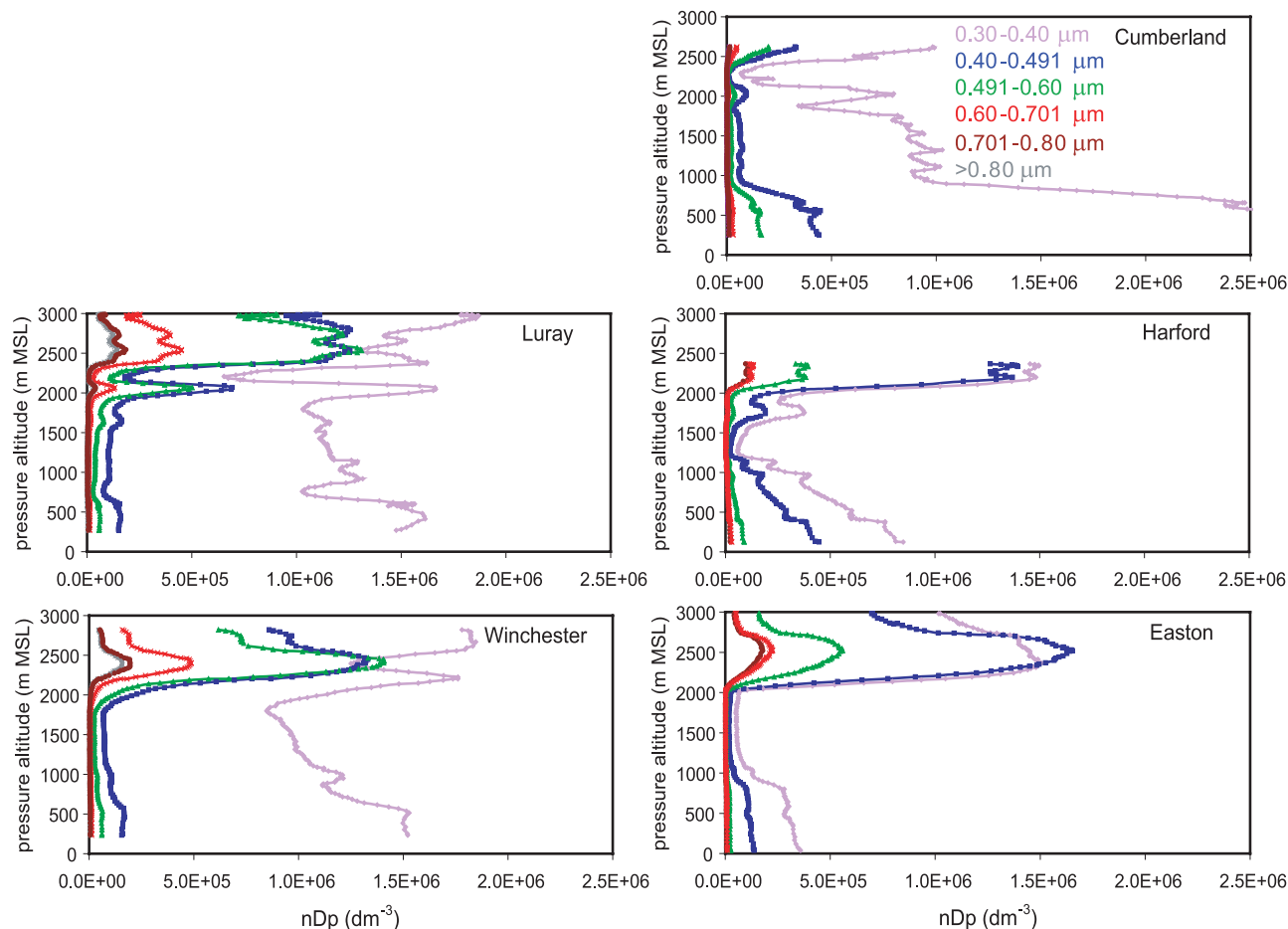


**Figure 11.** Number of particles in six discrete particle diameter size bins measured during the vertical survey spirals over Luray, Winchester, Cumberland, Harford, and Easton: 0.30–0.40  $\mu\text{m}$  (violet), 0.40–0.491  $\mu\text{m}$  (blue), 0.491–0.60  $\mu\text{m}$  (green), 0.60–0.701  $\mu\text{m}$  (red), 0.701–0.80  $\mu\text{m}$  (maroon), 0.80–1.0  $\mu\text{m}$  (gray).

wavelengths were then calculated based on the size distributions and wavelength-dependent complex indices of refraction.

### 3.5. Aerosol Direct Radiative Forcing

[30] The clear-sky aerosol direct radiative forcing ( $\Delta F$ ) at each location was calculated using the Santa Barbara DISORT Radiative Transfer (SBDART) code [Ricchiuzzi *et al.*, 1998]. AOD is proportional to the sum of the scattering and absorption cross sections calculated from Mie theory, allowing measured values to be extrapolated to any wavelength. The calculated values of AOD and  $\omega_0$  at 0.30, 0.40, 0.55, 0.70, 1.0, 2.0, and 3.0  $\mu\text{m}$  in  $\sim 100$  m vertical layers from roughly the surface to 3 km (depending on the vertical survey spiral at each location) were used as inputs to the code. Measured temperature, pressure, water vapor, and ozone values were also input for the lowest 3 km. Surface albedo between 0.47–2.1  $\mu\text{m}$  was taken from the MODIS land team 8 day surface reflectance product [Vermote and Vermuelen, 1999] (see [http://modis.gsfc.nasa.gov/data/atbd/atbd\\_mod08.pdf](http://modis.gsfc.nasa.gov/data/atbd/atbd_mod08.pdf)), derived from satellite measurements during a low-aerosol period 2–3 weeks after this study. Outside of this wavelength range, CERES mixed vegetation albedos were used (T. Charlock *et al.*, 2002, <http://www-surf.larc.nasa.gov/surf/pages/explan.html>). These values were cho-

sen because of consistency with the MODIS land team surface reflectance at the specified sites.

[31]  $\Delta F$  TOA,  $\Delta F$  sfc, and atmospheric absorption (Atmos) were calculated at each location. To determine the effects of the smoke layer at each location, the program was run with the smoke layer intact and after removal of the layer. The difference between the two sets of outputs was the direct effect of the smoke plume (Table 4). The PBL forcing was compared to a zero aerosol background and was, therefore, not the anthropogenic forcing. Since no background was assumed, a more accurate value for the smoke forcing was thereby obtained. Because the smoke signature was weak at Cumberland and the majority of the plume was not measured at Harford, the values reported for these locations are not necessarily representative of the situation being described.

[32] Sources of error in the values calculated using the radiative transfer code resulted from uncertainties in the AOD at 550 nm and the extrapolation to other wavelengths using Mie theory. The AOD at 550 nm was found to be linearly proportional to the calculated forcing values, and the uncertainty in the forcing values was therefore assumed to be proportional to the uncertainty in AOD. The extrapolation uncertainty was calculated using sensitivity tests in which the real index of refraction was varied by 0.04

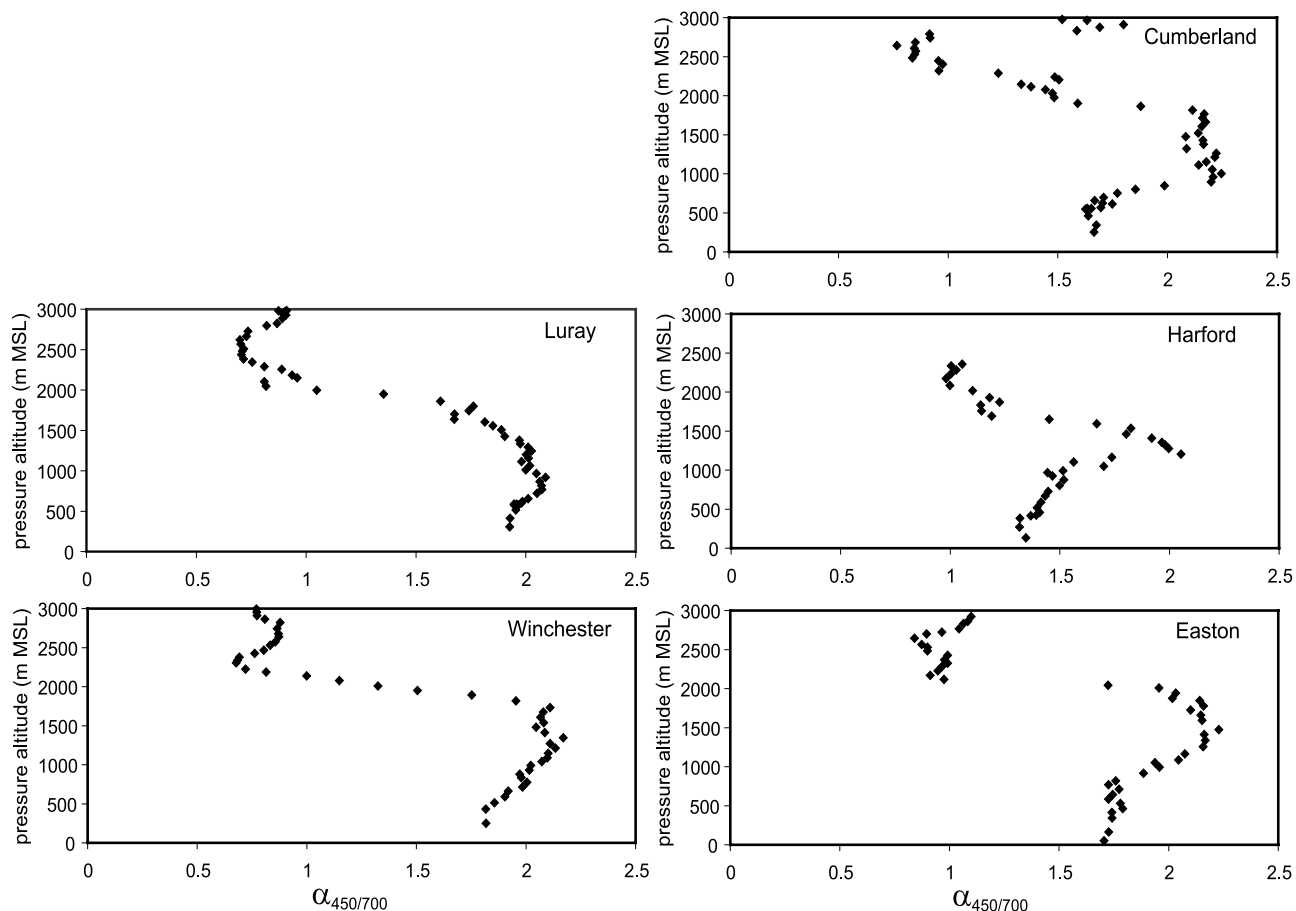


**Figure 12.** Scattering Ångström exponent,  $\alpha_{450/700}$ , calculated from flight data measured during the vertical survey spirals over Luray, Winchester, Cumberland, Harford, and Easton.

(a value greater than the AERONET uncertainty of 0.03) [Dubovik *et al.*, 2000], and the Ångström exponents used to calculate the size distributions were varied by one standard deviation. These sources of error were then added in quadrature to give the uncertainties listed in Table 4.

[33] Calculations of the effect of the smoke plume indicated that the forcing at the TOA was small relative to the surface forcing. The values for atmospheric absorption were, therefore, nearly equal to the attenuation at the surface. This indicates that multiple scattering of solar radiation within the optically thick plume typically ended in photon absorption. The fact that the smoke overlaid more scattering, smaller particles also increased the absorption

within the smoke layer. The net effect was to cool the surface and heat the air aloft, thereby increasing the vertical stability of the lower atmosphere.

[34] To quantify this effect, the calculated heating rates at each spiral location were integrated from sunrise to the time of observation. These values were then used to generate vertical heating profiles. Observed temperature profiles from the surface to  $\sim 2$  km (below the temperature inversion) were extrapolated to 3 km to provide a temperature profile that did not include the observed inversion. The extrapolated temperature profiles were then subtracted from the measured temperature profiles. The resulting temperature difference was compared to the

**Table 1.** Ångström Exponents Calculated for the Smoke Layer and Planetary Boundary Layer (PBL) at Vertical Survey Spiral Locations During Flights on 8 July 2002<sup>a</sup>

	Smoke			PBL		
	$\alpha_{450/550}$	$\alpha_{450/700}$	$\alpha_{550/700}$	$\alpha_{450/550}$	$\alpha_{450/700}$	$\alpha_{550/700}$
Luray	$0.57 \pm 0.18$	$0.83 \pm 0.15$	$1.04 \pm 0.11$	$1.84 \pm 0.42$	$1.92 \pm 0.38$	$1.99 \pm 0.34$
Winchester	$0.60 \pm 0.44$	$0.85 \pm 0.32$	$1.05 \pm 0.22$	$1.90 \pm 0.34$	$1.99 \pm 0.32$	$2.06 \pm 0.30$
Cumberland	$1.17 \pm 0.64$	$1.23 \pm 0.38$	$1.29 \pm 0.30$	$1.85 \pm 0.26$	$1.96 \pm 0.22$	$2.05 \pm 0.21$
Harford	$0.87 \pm 0.10$	$1.09 \pm 0.09$	$1.26 \pm 0.09$	$1.45 \pm 0.33$	$1.59 \pm 0.30$	$1.70 \pm 0.29$
Easton	$0.71 \pm 0.10$	$0.97 \pm 0.09$	$1.18 \pm 0.09$	$1.83 \pm 0.19$	$1.94 \pm 0.19$	$2.03 \pm 0.16$

<sup>a</sup>Uncertainties represent 1  $\sigma$  deviation about the mean.

**Table 2.** Aerosol Optical Depth (AOD) at 550 nm Calculated From ~5 m Above Ground Level to ~3 km Above Mean Sea Level at Vertical Survey Spiral Locations During Flights on 8 July 2002

	Luray	Winchester	Cumberland	Harford <sup>a</sup>	Easton
$\tau_{550}$	$1.01 \pm 0.14$	$0.98 \pm 0.14$	$0.42 \pm 0.06$	$1.05 \pm 0.15$	$1.53 \pm 0.21$

<sup>a</sup>Aerosol optical depth only to ~2.5 km above mean sea level.

integrated heating profiles to determine the impact of the absorptive heating on the observed temperature profiles (Figure 14).

[35] The integrated heating for the morning profiles underestimated the observed temperature difference while the afternoon profiles overestimated the amount of heating. The spatially and temporally dynamic nature of the smoke plume would naturally affect the accuracy of this calculation. However, there was also more smoke above the highest measurements made in the aircraft, which was unaccounted for in the heating rate calculations. Solar attenuation from this unaccounted for smoke would reduce the calculated absorption, and thereby the heating rates, at lower altitudes. This would decrease the amplitude and width of the resulting heating rate profiles. Although these explanations could account for the discrepancy in the afternoon profiles, heating in the smoke layer did not seem to account for the morning inversion.

**Table 3.** Single-Scattering Albedo at 550 nm Calculated for the Smoke Layer and PBL at Vertical Survey Spiral Locations During Flights on 8 July 2002

	Luray	Winchester	Cumberland	Harford	Easton
Smoke ( $\omega_{0_{550}}$ )	$0.91 \pm 0.03$	$0.93 \pm 0.02$	$0.81 \pm 0.06$	$0.93 \pm 0.02$	$0.93 \pm 0.02$
PBL ( $\omega_{0_{550}}$ )	$0.95 \pm 0.01$	$0.95 \pm 0.01$	$0.94 \pm 0.02$	$0.94 \pm 0.02$	$0.96 \pm 0.01$

[36] Figure 15 is the NOAA ARL EDAS meteogram of pressure vertical velocity from 900–700 mb, which shows weak subsidence on the morning of 8 July. Hence adiabatic heating of the descending air may have initially capped the mixed layer and positioned the smoke plume in a thin layer just above it, where heating of the absorptive smoke layer strengthened the inversion. The meteogram shows negative vertical velocity beginning at ~1500 UTC, indicating upward vertical motion. If the modeled vertical velocity was correct, the subsidence inversion should have dissipated by the afternoon. However, the measured temperature showed an inversion after 2000 UTC. Thus the initial subsidence inversion may have acted to sequester the smoke in a thin enough layer above the PBL where it heated the layer and stabilized the atmosphere enough to create a positive feedback loop for its own sequestration. This

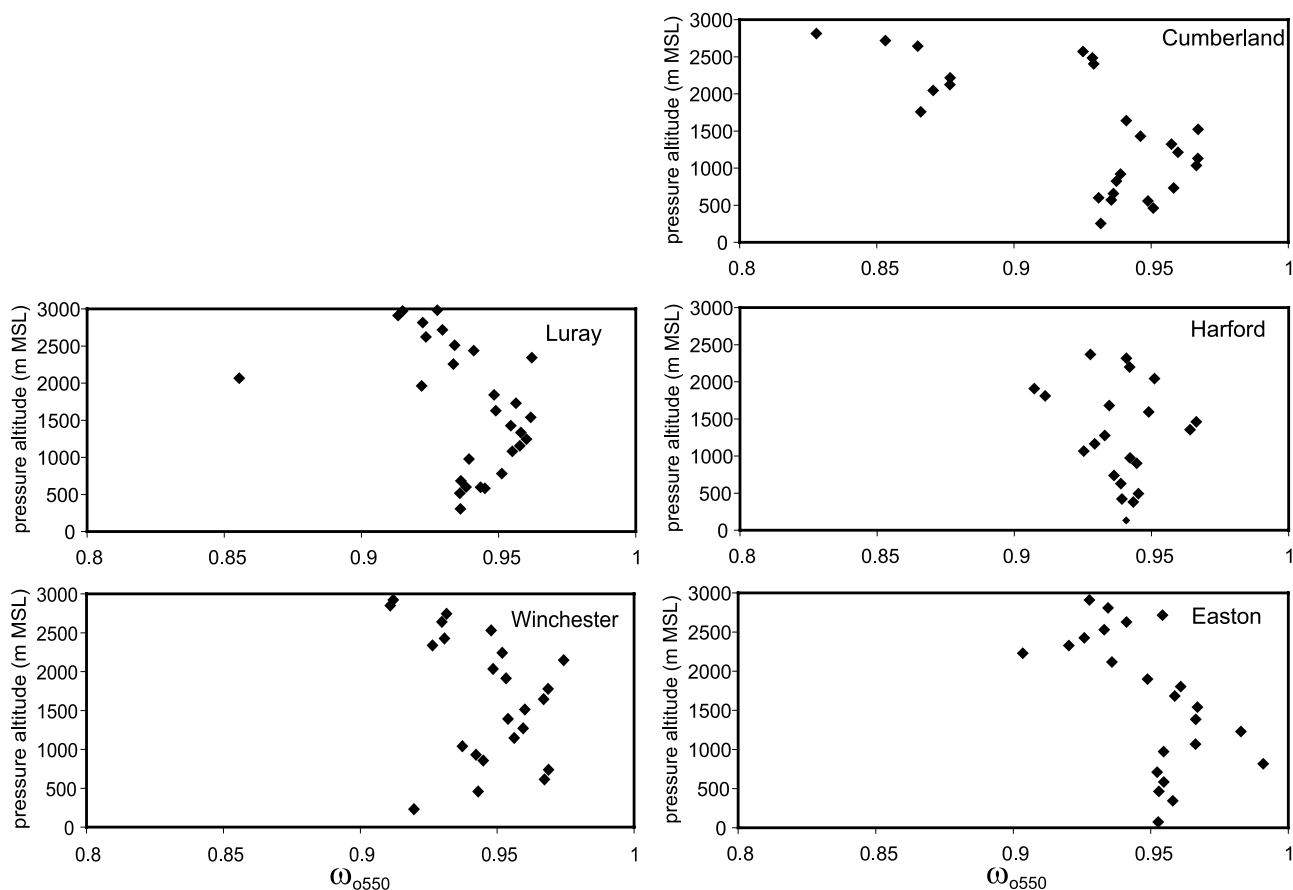


**Figure 13.** Single-scattering albedo,  $\omega_0$ , at 550 nm, calculated from flight data measured during the vertical survey spirals over Luray, Winchester, Cumberland, Harford, and Easton.

**Table 4.** Top of the Atmosphere Forcing ( $\Delta F$  TOA), Surface Forcing ( $\Delta F$  sfc), and Atmospheric Absorption (Atmos) Calculated at Vertical Survey Spiral Locations During Flights on 8 July 2002

	Total Forcing <sup>a</sup>			PBL <sup>b</sup>			Smoke <sup>c</sup>		
	$\Delta F$ TOA, $\text{Wm}^{-2}$	Atmos, $\text{Wm}^{-2}$	$\Delta F$ sfc, $\text{Wm}^{-2}$	$\Delta F$ TOA, $\text{Wm}^{-2}$	Atmos, $\text{Wm}^{-2}$	$\Delta F$ sfc, $\text{Wm}^{-2}$	$\Delta F$ TOA, $\text{Wm}^{-2}$	Atmos, $\text{Wm}^{-2}$	$\Delta F$ sfc, $\text{Wm}^{-2}$
Luray	$-47 \pm 7$	$115 \pm 17$	$-162 \pm 24$	$-26 \pm 4$	$30 \pm 5$	$-56 \pm 8$	$-21 \pm 3$	$85 \pm 13$	$-106 \pm 16$
Winchester	$-50 \pm 8$	$108 \pm 16$	$-168 \pm 25$	$-20 \pm 3$	$23 \pm 3$	$-43 \pm 6$	$-30 \pm 5$	$85 \pm 13$	$-115 \pm 17$
Cumberland	$-25 \pm 4$	$57 \pm 9$	$-82 \pm 12$	$-27 \pm 4$	$36 \pm 5$	$-63 \pm 9$	$2 \pm 1$	$21 \pm 3$	$-19 \pm 3$
Harford	$-42 \pm 6$	$124 \pm 19$	$-166 \pm 25$	$-31 \pm 5$	$57 \pm 9$	$-88 \pm 13$	$-11 \pm 2$	$67 \pm 10$	$-78 \pm 12$
Easton	$-57 \pm 9$	$167 \pm 25$	$-224 \pm 34$	$-29 \pm 4$	$29 \pm 4$	$-58 \pm 9$	$-28 \pm 4$	$138 \pm 21$	$-166 \pm 25$

<sup>a</sup>Calculated with the PBL and smoke layers.

<sup>b</sup>Calculated with just the PBL layer.

<sup>c</sup>Difference between the total forcing and PBL values.

prevented vertical mixing and dilution and ultimately increased the regional impact of the plume.

#### 4. Conclusions

[37] Measurements were made of trace gas and particle concentrations as well as particle optical properties associ-

ated with the smoke plume advected  $\sim 1500$  km from Quebec forest fires. Large increases in CO and O<sub>3</sub> mixing ratios, total particle scattering and absorption, as well as in the number of particles with optical diameters between  $0.30 \sim 1.0 \mu\text{m}$  were observed between  $\sim 2$  and  $3$  km. However, very little SO<sub>2</sub> (less than 0.1% of the CO) was observed at this altitude.

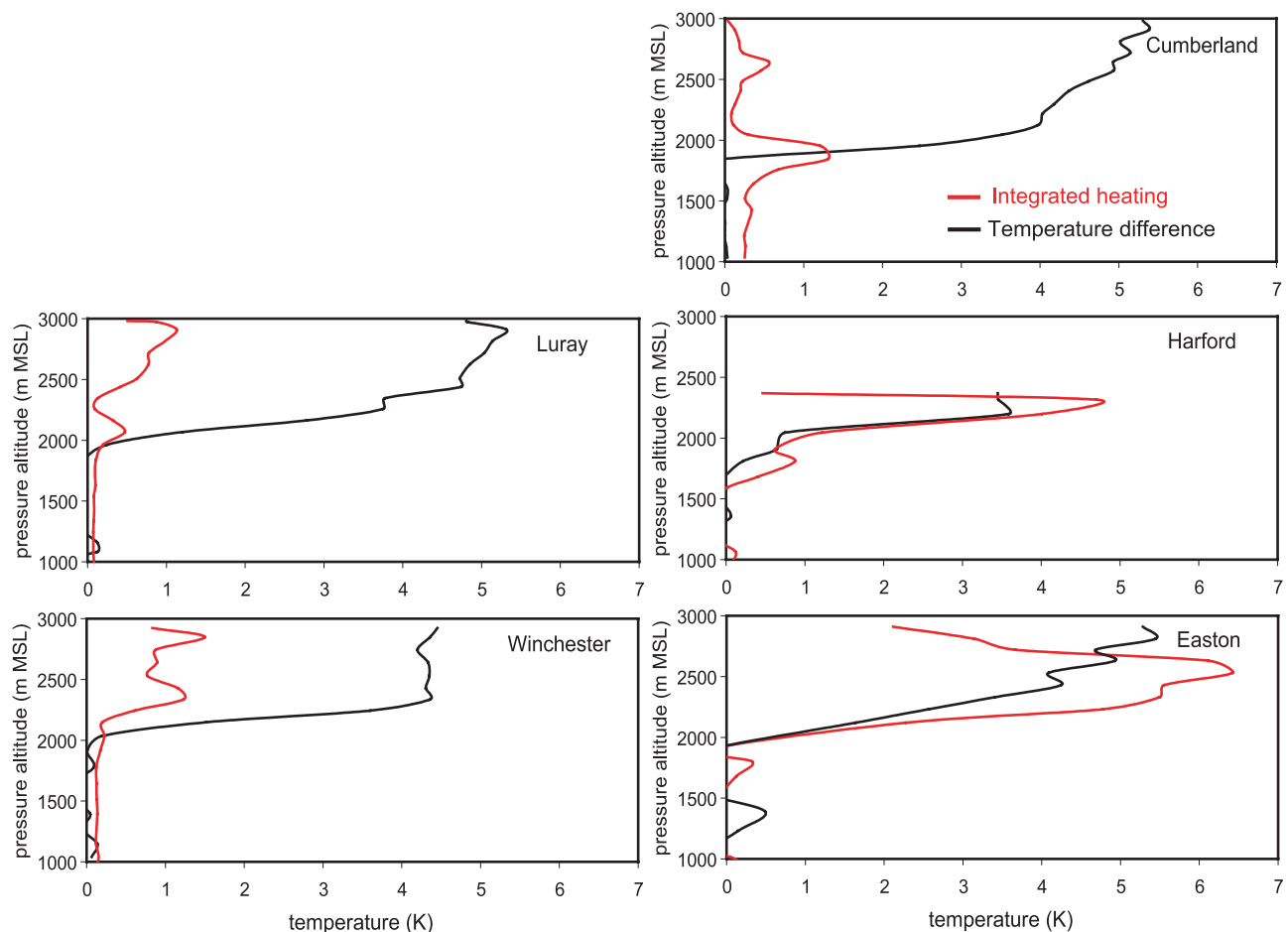


**Figure 14.** Temperature differences between the temperature measured during the vertical survey spirals over Luray, Winchester, Cumberland, Harford, and Easton and temperature profiles extrapolated from 2 to 3 km as if there were no temperature inversions, shown with the black lines. The integrated heating profiles calculated with the radiative transfer code and integrated from sunrise to the time of each observation spiral are given with the red lines.

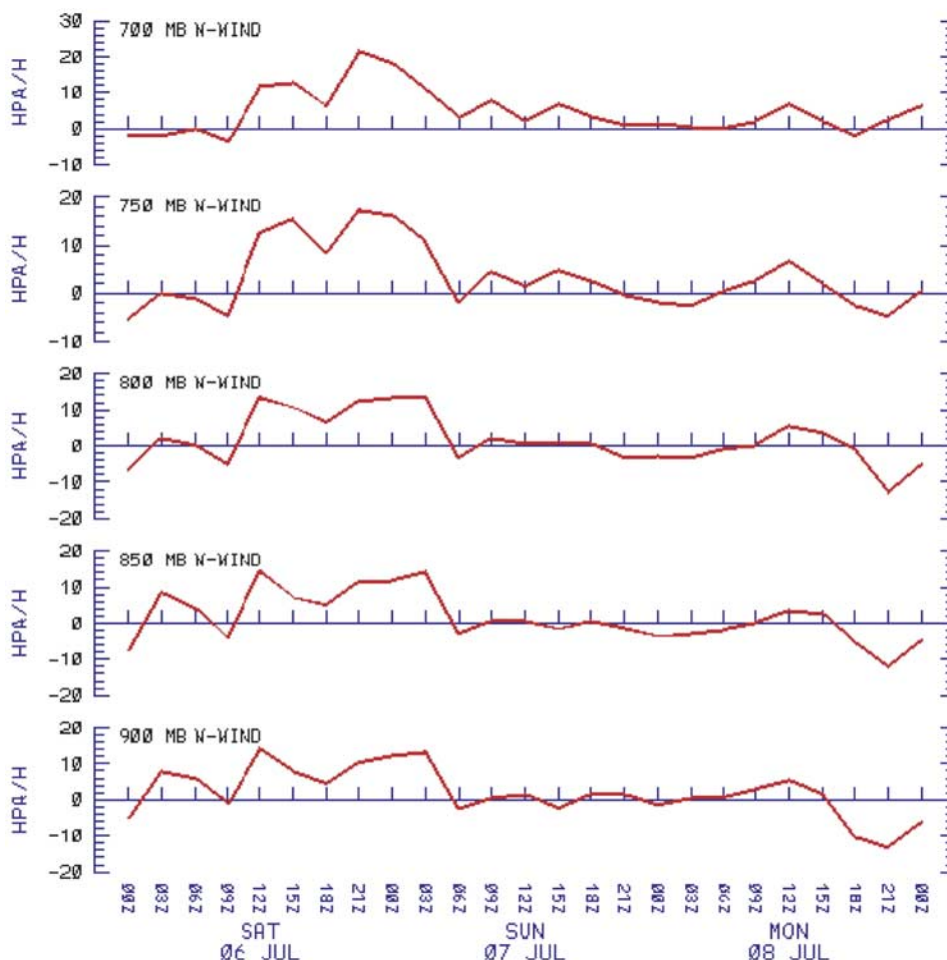


**Figure 15.** NOAA ARL EDAS meteogram of the pressure vertical velocity at 39.18°N, 76.67°W for 6–8 July 2002. The morning of 8 July shows downward vertical motion. By the afternoon of 8 July, there is upward vertical motion.

[38] The more absorptive smoke particles had a mean single-scattering albedo value of  $0.93 \pm 0.02$  at 550 nm while the underlying PBL particles had a mean value of  $0.95 \pm 0.01$  at 550 nm. The scattering Ångström exponents of the larger, aged smoke particles were between  $0.83 \pm 0.15$  and  $1.23 \pm 0.38$  while the smaller, PBL particles had values between  $1.59 \pm 0.30$  and  $1.99 \pm 0.32$  for  $\alpha_{450/700}$ . Calculated aerosol optical depths (550 nm) from just above the surface to  $\sim 3$  km ranged from  $0.42 \pm 0.06$  above Cumberland to  $1.53 \pm 0.21$  above Easton.

[39] Clear-sky aerosol direct radiative forcing was calculated at each location using the SBDART code. Absorption of solar radiation within the smoke plume nearly equaled that which was attenuated at the surface, acting to cool the surface and heat the air aloft. Owing to a morning subsidence inversion, the smoke plume was positioned in a thin layer above the PBL between  $\sim 2$  and 3 km. The heating of this layer was concentrated enough to maintain the temperature inversion through the afternoon. This created a positive feedback loop that prevented vertical mixing and dilution, thereby protracting the lifetime of the plume and the regional radiative impacts.

[40] **Acknowledgments.** Funding for this work was provided by the Maryland Department of Environment (MDE), the Mid-Atlantic and Northeast-Visibility Union (MANE-VU), and the U.S. Department of Energy's Atmospheric Radiation Measurement (ARM) program, grant DEFG0201ER63166. The authors are eternally grateful to the AERONET team and to Paul Ricchiazzi and the SBDART code. We gratefully acknowledge the NOAA Air Resources Laboratory (ARL) for the provision of the HY-SPLIT transport and dispersion model and/or READY website (<http://www.arl.noaa.gov/ready.html>) used in this publication. We would like to thank the MODIS rapid response system team for their image of the smoke plume. A special thanks for their support and contributions goes to Tad Abum, George Allen, Kevin Civerolo, Tom Downs, Rich Poirot, Matt Seybold, Gopal Sistla, Jeff Stehr, and Jeff Underhill.

## References

- Anderson, T. L., and J. A. Ogren (1998), Determining aerosol radiative properties using the TSI 3563 Integrating Nephelometer, *Aerosol Sci. Technol.*, **29**, 57–69.
- Anderson, T. L., et al. (1996), Performance characteristics of a high-sensitivity, three-wavelength, total scatter/backscatter nephelometer, *J. Atmos. Oceanic Technol.*, **13**, 967–986.
- Anderson, T. L., D. S. Covert, J. D. Wheeler, J. M. Harris, K. D. Perry, B. E. Trost, and D. J. Jaffe (1999), Aerosol backscatter fraction and single scattering albedo: Measured values and uncertainties at a coastal station in the Pacific Northwest, *J. Geophys. Res.*, **104**, 26,793–26,807.
- Anderson, T. L., S. J. Masonis, D. S. Covert, N. C. Ahlquist, S. G. Howell, A. D. Clarke, and C. S. McNaughton (2003), Variability of aerosol optical properties derived from in situ aircraft measurements during ACE-Asia, *J. Geophys. Res.*, **108**(D23), 8647, doi:10.1029/2002JD003247.

- Andreae, M. O., and P. Merlet (2001), Emission of trace gases and aerosols from biomass burning, *Global Biogeochem. Cycles*, *15*, 955–966.
- Bodhaine, B. A. (1995), Aerosol absorption measurements at Barrow, Mauna Loa, and the South Pole, *J. Geophys. Res.*, *100*, 8967–8975.
- Bond, T. C., T. L. Anderson, and D. Campbell (1999), Calibration and intercomparison of filter-based measurements of visible light absorption by aerosols, *Aerosol Sci. Technol.*, *30*, 582–600.
- Chang, H., and T. Charalampopoulos (1990), Determination of the wavelength dependence of refractive indices of flame soot, *Proc. R. Soc. London*, *430*, 577–591.
- Charlson, R. J., J. Langner, H. Rodhe, C. B. Leovy, and S. G. Warren (1991), Perturbation of the Northern-Hemisphere radiative balance by backscattering from anthropogenic sulfate aerosols, *Tellus, Ser. A*, *43*, 152–163.
- Crutzen, P. J., and M. O. Andreae (1990), Biomass burning in the tropics—Impact on atmospheric chemistry and biogeochemical cycles, *Science*, *250*, 1669–1678.
- Crutzen, P. J., L. E. Heidt, J. P. Krasnek, W. H. Pollock, and W. Seiler (1979), Biomass burning as a source of atmospheric gases CO, H<sub>2</sub>, N<sub>2</sub>O, NO, CH<sub>3</sub>Cl and COS, *Nature*, *282*, 253–256.
- Delmas, R. (1982), On the emission of carbon, nitrogen and sulfur in the atmosphere during bushfires in intertropical savannah zones, *Geophys. Res. Lett.*, *9*, 761–764.
- Dickerson, R. R., and A. C. Delany (1988), Modification of a commercial gas filter correlation CO detector for increased sensitivity, *J. Atmos. Oceanic Technol.*, *5*(3), 424–431.
- Doddridge, B. G., P. C. Novelli, and R. M. Rosson (1995), WMO meeting of experts on global carbon monoxide measurements, in *Rapporteur's Report of the Working Session on Measurement Techniques and Standards*, pp. 8–11, World Meteorol. Organ., Boulder, Colo.
- Dubovik, O., A. Smirnov, B. N. Holben, M. D. King, Y. J. Kaufman, T. F. Eck, and I. Slutsker (2000), Accuracy assessments of aerosol optical properties retrieved from Aerosol Robotic Network (AERONET) Sun and sky radiance measurements, *J. Geophys. Res.*, *105*, 9791–9806.
- Dubovik, O., B. N. Holben, T. F. Eck, A. Smirnov, Y. J. Kaufman, M. D. King, D. Tanre, and I. Slutsker (2001), Variability of absorption and optical properties of key aerosol types observed in worldwide locations, *J. Atmos. Sci.*, *59*, 590–608.
- Eck, T. F., B. N. Holben, I. Slutsker, and A. Setzer (1998), Measurements of irradiance attenuation and estimation of aerosol single-scattering albedo for biomass burning aerosols in Amazonia, *J. Geophys. Res.*, *103*, 31,865–31,878.
- Evans, L. F., I. A. Weeks, A. J. Eccleston, and D. R. Packham (1977), Photochemical ozone in smoke from prescribed burning of forests, *Environ. Sci. Technol.*, *11*, 896–900.
- Ferrare, R. A., R. S. Fraser, and Y. J. Kaufman (1990), Satellite measurement of large-scale air pollution measurements of forest fire smoke, *J. Geophys. Res.*, *95*, 9911–9925.
- Hobbs, P. V., J. S. Reid, R. A. Kotchenruther, R. J. Ferek, and R. Weiss (1997), Direct radiative forcing by smoke from biomass burning, *Science*, *275*, 1776–1778.
- Holben, B. N., et al. (1998), AERONET—A federated instrument network and data archive for aerosol characterization, *Remote Sens. Environ.*, *66*, 1–16.
- Li, Z. (1998), Influence of absorbing aerosols on the inference of solar surface radiation budget and cloud absorption, *J. Clim.*, *11*, 5–17.
- Li, Z., and L. Kou (1998), Atmospheric direct radiative forcing by smoke aerosols determined from satellite and surface measurements, *Tellus, Ser. B*, *50*, 543–554.
- Luke, W. T. (1997), Evaluation of a commercial pulsed fluorescence detector for the measurement of low-level SO<sub>2</sub> concentrations during the Gas-Phase Sulfur Intercomparison Experiment, *J. Geophys. Res.*, *102*, 16,255–16,265.
- Martins, J. V., P. Artaxo, C. Liousse, J. S. Reid, P. V. Hobbs, and Y. J. Kaufman (1998), Effects of black carbon content, particle size, and mixing on light absorption by aerosols from biomass burning in Brazil, *J. Geophys. Res.*, *103*, 32,041–32,050.
- McKee, S. A., G. Wotawa, D. D. Parrish, J. S. Holloway, M. P. Bühr, G. Hübler, F. C. Fehsenfeld, and J. F. Meagher (2002), Ozone production from Canadian wildfires during June and July of 1995, *J. Geophys. Res.*, *107*(D14), 4192, 10.1029/2001JD000697.
- Mishchenko, M. I., L. D. Travis, and A. A. Lacis (2002), *Scattering, Absorption, and Emission of Light by Small Particles*, Cambridge Univ. Press, New York.
- Novelli, P. C., et al. (1998), An internally consistent set of globally distributed atmospheric carbon monoxide mixing ratios developed using results from an intercomparison of measurements, *J. Geophys. Res.*, *103*, 19,285–19,293.
- Park, R. J., G. L. Stenchikov, K. E. Pickering, R. R. Dickerson, D. J. Allen, and S. Kondragunta (2001), Regional air pollution and its radiative forcing: Studies with a single-column chemical and radiation transport model, *J. Geophys. Res.*, *106*, 28,751–28,770.
- Penner, J. E., R. E. Dickinson, and C. A. O'Neill (1992), Effects of aerosol from biomass burning on the global radiation budget, *Science*, *256*, 1432–1434.
- Ramanathan, V., P. J. Crutzen, J. T. Kiehl, and D. Rosenfeld (2001), Aerosols, climate, and the hydrological cycle, *Science*, *294*, 2119–2123.
- Reid, J. S., P. V. Hobbs, R. J. Ferek, D. R. Blake, J. V. Martins, J. V. Dunlap, and C. Liousse (1998), Physical, chemical, and optical properties of regional hazes dominated by smoke in Brazil, *J. Geophys. Res.*, *103*, 32,059–32,080.
- Reid, J. S., T. F. Eck, S. A. Christopher, P. V. Hobbs, and B. Holben (1999), Use of the Angstrom exponent to estimate the variability of optical and physical properties of aging smoke particles in Brazil, *J. Geophys. Res.*, *104*, 27,473–27,489.
- Remer, L. A., S. Gassó, D. A. Hegg, Y. J. Kaufman, and B. N. Holben (1997), Urban/industrial aerosol: Ground-based Sun/sky radiometer and airborne in situ measurements, *J. Geophys. Res.*, *102*, 16,849–16,859.
- Remer, L. A., Y. J. Kaufman, B. N. Holben, A. M. Thompson, and D. McNamara (1998), Biomass burning aerosol size distribution and modeled optical properties, *J. Geophys. Res.*, *103*, 31,879–31,891.
- Ricchiazzi, P., S. Yang, D. Gautier, and D. Sowle (1998), SBDART: A research and teaching software tool for plane-parallel radiative transfer in the Earth's atmosphere, *Bull. Am. Meteorol. Soc.*, *79*, 2101–2114.
- Ryan, W. F., B. G. Doddridge, R. R. Dickerson, R. M. Morales, K. A. Hallock, P. T. Roberts, D. L. Blumenthal, J. A. Anderson, and K. L. Civerolo (1998), Pollutant transport during a regional O<sub>3</sub> episode in the Mid-Atlantic states, *J. Air Waste Manage. Assoc.*, *48*, 786–797.
- Stith, J. L., F. R. Lawrence, and P. V. Hobbs (1981), Particle emissions and the production of ozone and nitrogen-oxides from the burning of forest slash, *Atmos. Environ.*, *15*, 73–82.
- Vermote, E., and E. Vermuelen (1999), Atmospheric correction algorithm: Spectral reflectances (MOD09), algorithm theoretical basis document, NASA, Greenbelt, Md.
- Wong, J., and Z. Li (2002), Retrieval of optical depth for heavy smoke aerosol plumes: Uncertainties and sensitivities to the optical properties, *J. Atmos. Sci.*, *59*, 250–261.
- R. R. Dickerson, B. G. Doddridge, Z. Li, L. T. Marufu, C. A. Piety, and B. L. Vant-Hull, Department of Meteorology, 2335 Computer and Space Sciences Building, University of Maryland, College Park, MD 20742, USA. (russ@atmos.umd.edu; bruce@metosrv2.umd.edu; zli@atmos.umd.edu; marufu@atmos.umd.edu; charles@atmos.umd.edu; brianvh@atmos.umd.edu)
- B. F. Taubman, Department of Chemistry, University of Maryland, 2107 Computer and Space Sciences Building, College Park, MD 20742, USA. (btaubman@atmos.umd.edu)